Thermally induced coloration of KBr at high pressures

Sarah M. Arveson, Boris Kiefer, Jie Deng, Zhenxian Liu, and Kanani K. M. Lee

1   **Thermally-induced coloration of KBr at high pressures**

2   Sarah M. Arveson[1*], Boris Kiefer[2], Jie Deng[1], Zhenxian Liu[3] and Kanani K. M. Lee[1]

3   [1]*Department of Geology & Geophysics, Yale University, New Haven CT 06511*

4   [2]*Department of Physics, New Mexico State University, Las Cruces NM 88011*

5   [3]*Department of Civil and Environmental Engineering, The George Washington*

6   *University, Washington DC 20052*

7   [*]Corresponding author

8   (Dated February 12, 2018)

9

10   **Abstract**

11   Laser-heated diamond-anvil cell (LHDAC) experiments reveal electronic changes

12   in KBr at pressures between ~13-81 GPa when heated to high temperatures that cause

13   runaway heating to temperatures in excess of ~5000 K. The drastic changes in absorption

14   behavior of KBr are interpreted as rapid formation of high-pressure F-center defects. The

15   defects are localized to the heated region and thus do not change the long-range

16   crystalline order of KBr. The results have significant consequences for temperature

17   measurements in LHDAC experiments and extend the persistence of F-centers in alkali

18   halides to at least 81 GPa.

19

20

21

22

23

I. INTRODUCTION

The existence of defects in alkali halides under irradiation is well documented.[1,2] High-intensity x-ray, UV, and infrared irradiation can generate defects that color nominally transparent alkali halides. The most prevalent color centers in KBr are F-centers, which consist of an electron trapped in a Br vacancy. Models for the radiation damage process in alkali halides include formation of F-centers, aggregation of defect clusters, extended defect formation, and finally annealing, when the defects decay and return to their pre-irradiated condition.[2] Extensive work at 300 K and below has been conducted to characterize the structure, properties, and timescales of defects during these stages. However, only a few studies have explored the effect of high temperatures or high pressures on color centers in alkali halides, and they have been limited to pressures < 17 GPa.[3-6] In these studies, defects were introduced into the samples by irradiation prior to applying pressure.

We report experimental evidence for reversible defect formation in polycrystalline KBr at high pressures (13-81 GPa) and temperatures (>5000 K) using infrared laser heating that turns the initially transparent KBr opaque. KBr is an insulator with a band-gap of 7.6 eV,[3] too large for direct electronic excitations from the valence band into the conduction band with infrared or visible light. However, F-centers acting as electron donors cause electronic states in the band-gap that affect optical properties and, in particular, absorption and emission characteristics. Defect-related electronic changes are important for characterizing material performance, as KBr is used widely in optical devices. F-centers in salts under planetary conditions may allow novel characterization of planetary and lunar surfaces.[7] Changes in absorption behavior are also crucial to

47 temperature measurements in LHDAC experiments which often use KBr and other alkali

48 halides as insulation media.[4]

49

II. METHODS

A. Sample Preparation

52   Single crystal KBr (Intl. Crystal Laboratories, 99.95% purity) was ground up into

53 a fine polycrystalline mixture, and a 10-20 μm thick disk was loaded into a rhenium-

54 gasketted diamond-anvil cell with a small amount of metal foil as a laser absorber. We

55 performed several sets of experiments using Pt, Fe, stoichiometric FeSi, or an Fe-Si9wt%

56 alloy to ensure independence of the KBr behavior regardless of metal laser absorber.

57 Great care was taken to prevent contamination of the samples, including drying the

58 assemblies in an oven to minimize surface hydration. Prior to applying pressure, the

59 LHDAC was placed in an oven at 400 K for at least 1 hour to minimize moisture in the

60 sample chamber. We found that runaway heating and defect formation occur regardless

61 of whether an assembly is dried under vacuum for 1 hour or 10 days. Pressure was

62 calibrated using the high-frequency edge of the diamond Raman band [8] or the equation

63 of state of KBr [9] for the x-ray diffraction experiments. See Table I for individual

64 sample details.

65

B. Laser Heating

67   To generate defects in KBr, we performed high-pressure experiments in the

68 LHDAC using a 1070 nm (~1.16 eV) fiber CW laser. The sample is subjected to either

69 steady heating at a peak power or single-sided predefined ramp heating [10] on the KBr-

70   side, in which the sample is annealed at a low laser power and subsequently ramped to a

71   peak power until the laser is shut off (Table I). We positioned the laser on the edge of the

72   metal foil during heating and collected a two-dimensional temperature map at the peak

73   temperature using the 4-color method.[10] Details on temperature measurement and

74   accuracy can be found in Ref. 10. To avoid damage to the diamonds, once the KBr begins

75   absorbing the laser and thermally runs away, it remains at the peak temperature for no

76   more than 0.3 s before the sample is temperature quenched by shutting off the laser,

77   which takes < 1 μs.

78

79   **C. Characterization Techniques**

80   High-pressure optical absorption measurements between 450 nm and 1000 nm

81   were conducted at the Infrared Lab of the National Synchrotron Light Source II at

82   Brookhaven National Laboratory after temperature quenching. The visible absorption

83   spectra were collected through a customized visible microscope system together with a

84   spectrograph (SpectraPro SP-2556, Princeton Instruments) and a liquid nitrogen cooled

85   PyLoN CCD detector. A reference spectrum was taken through an adjustable IRIS

86   aperture at unheated and transparent KBr area at each pressure.

87   High-pressure synchrotron mid-IR transmission and reflection measurements

88   were performed at beamline 1.4.3 of the Advanced Light Source, Lawrence Berkeley

89   National Laboratory after temperature quenching. The IR spectra with 4 cm^{-1} spectral

90   resolution were acquired through a Nicolet Magna 760 FTIR spectrometer and a custom

91   high-pressure IR microscope system.

92   We collected in-situ x-ray diffraction spectra of a 68 GPa KBr sample as defect

93   formation occurred. Spectra were taken at Sector 16-ID-B of the Advanced Photon

94   Source at Argonne National Lab using an x-ray wavelength 0.4066 Å.[11] Samples were

95   laser heated to a peak power of ~100 W and diffraction spectra were taken before, during,

96   and after heating while at pressure and upon decompression.

97   Raman spectra were taken with a Horiba-Jobin Yvon HR-800 Raman microscope

98   equipped with a 50-mW green laser (532 nm) with an 1800 lines/mm grating. In order to

99   avoid signal from the diamond anvils, spectra were taken between $100 - 1200$ cm^{-1}.

100

101   **D. Density Functional Theory**

102   Three-dimensional periodic density functional theory (DFT) calculations were

103   performed using Vienna Ab-initio Simulation Package (VASP) [12,13] The electronic

104   exchange and correlation effects were described in the GGA-PBE.[14] The interactions

105   between atoms were described within the PAW method.[15,16] The results of this

106   approach have been shown to be of comparable accuracy to all electron calculations for a

107   wide range of different materials.[15] The core region cut-off radii (1 a_B = 0.529 Å) of

108   the PAW potentials were 2.8 a_B (core configuration $3s^2 3p^6 4s^1$) and 2.1 a_B (core

109   configuration $4s^2 4p^5$), for K and Br, respectively. A plane-wave cutoff energy E_{cut}=500

110   eV was applied throughout all calculations. F-center formation energies were computed

111   for the B1 phase at equilibrium and for the B2 phase at equilibrium (0 GPa) and 50 GPa.

112   Following previous work,[17] F-centers in B1 phase were modeled as 2x2x2 supercells

113   of the conventional unit cell (64 ions: $K_{32}Br_{32}$) on a 2x2x2 Γ-centered k-point grid.

114   Similarly, F-center formation energies for the B2 phase were obtained from 3x3x3

115   supercells (54 ions, $K_{27}Br_{27}$) also on a 2x2x2 Γ-centered k-point grid. All structural

116   optimizations were performed at constant pressure, and any energy contributions from

117   zero-point motion and thermal vibrations were neglected. F-centers were generated by

118   removing one Br per supercell, and explored through spin polarized calculations were

119   performed. Possible symmetry lowering due to F-center defect formation was allowed.

120   However, we find that during F-center formation, the symmetry of the stoichiometric

121   parent phase is preserved and local relaxation is minute. This finding is consistent with

122   our XRD observations, which do not show any evidence for structural deviations from

123   the defect-free B1 and B2 phases.

124   We use density functional theory (DFT) calculations to calculate predicted F-

125   center formation energies. As has been noted before,[18] the formation of F-centers is

126   favorable in an atmosphere of excess potassium. In order to take the chemical potential(s)

127   of the surrounding atmosphere (metal-rich) into account, we follow previous work:[17]

128   bromine was modeled in phase I (12x12x12 Γ-centered k-point grid) which is stable at

129   ambient pressure to at least 65 GPa [19] and potassium was modeled in its stable body-

130   centered cubic (bcc) phase (16x16x16 Γ-centered k-point grid). F-center crystals do not

131   carry a net charge, and their formation energy can be written as in Eqn. 1

132                    $$E_f = E_D - E_H + \mu_{Br} \qquad\qquad (1)$$

133   where E_D is the total energy (enthalpy) of the defective structure, E_H is the total energy

134   (enthalpy) of the defect free host supercell. The chemical potential of Br is given by μ_{Br}.

135   The conditions of thermodynamic equilibrium impose limits for the accessible range of

136   μ_{Br}: In order for KBr to be stable against decomposition we must satisfy Eqn. 2

137                    $$\mu_K + \mu_{Br} \geq E_{KBr(s)} \qquad\qquad (2)$$

138   where $E_{KBr(s)}$ is the energy (enthalpy) of the defect free host phase. Thus, the lower limit

139   of μ_{Br} is given by $\mu_{Br} \geq E_{KBr(s)} - \mu_K$ and μ_K is the total energy/enthalpy per atom of bcc

140   potassium. Following the same logic, we can obtain the corresponding expression for the

141   K-poor case. Using the total energies/enthalpies from our DFT computations we

142   computed defect formation energies (Table II). The results strongly suggest that the

143   formation of an F-center is endothermic but more favorable than K vacancy formation,

144   especially at high pressures. These results advocate for F-centers as the dominant defect

145   in KBr, especially at pressures that are representative of the pressure conditions of our

146   experiments. The energy source for F-center formation is provided by the high

147   temperatures (thermal energy) in our experiments.

148   The analysis of the electronic band structure shows that KBr is a wide direct-gap

149   insulator with $E_g = 4.3$ eV, similar to previous computations, $E_g = 4.0$ eV [20] and

150   significantly lower than experiment, $E_g = 7.4$ eV [21] to 7.6 eV.[22] However, we note

151   that even at the DFT level, energy differences between occupied and unoccupied states

152   are larger than the energy of visible light. Our GW0 computational setup follows

153   previous work [23] and improves the comparison between theory and experiment

154   significantly, KBr in B1 phase remains a direct gap insulator with $E_g = 7.3$ eV. In

155   contrast, we find that KBr in B2 phase is an indirect-gap insulator with a DFT gap of $E_g =$

156   3.9 eV at equilibrium and $E_g = 3.7$ eV at 50 GPa. The GW0 increases E_g to 6.6 eV and

157   6.2 eV at equilibrium and 50 GPa, respectively and confirms that the B2 phase is an

158   indirect gap insulator. Thus, KBr is expected to be optically transparent for visible light

159   in both the B1 and the B2 phases, as observed experimentally.

160   F-centers create paramagnetic centers with defect levels deep within the

161   fundamental gap of the host crystal.[17] The same work for NaCl in the B1 phase shows

162   that hybrid functionals increase the band-gap and shift the defect level deeper into the

163   band-gap (relative to the conduction band minimum). We find qualitatively similar

164   behavior in KBr: F-center separation from the conduction band minimum is 0.8 eV, 0.7

165   eV, 1.0 eV for B1 at equilibrium, B2 at equilibrium, and B2 at 50 GPa, respectively. Our

166   PBE0 computations show a similar pressure dependence (the amount of exact exchange

167   was adjusted such that the PBE0 [24] computations matched the GW0 computed

168   electronic structure: 38.7%, 36.0%, and 33.0% for B1 at equilibrium, B2 at equilibrium,

169   and B2 at 50 GPa, respectively). The respective F-center induced defect states with these

170   parameters are located 2.6 eV, 2.3 eV, and 3.2 eV below the conduction band minimum.

171   However, the exact location of the defect level and the inferred optical properties from

172   DFT and post-DFT computations must be considered uncertain even at equilibrium.[17]

173

174   **III. RESULTS AND DISCUSSION**

175   **A. Onset of Defect Formation**

176   Below a critical temperature, KBr insulates the metal and is transparent to the

177   infrared laser as in previous studies. At or above the critical temperature, near the

178   projected melting temperature of KBr,[25] the KBr absorbed the laser radiation directly,

179   leading to runaway temperatures in excess of 5500 K. Once runaway absorption from the

180   KBr began, the laser was shut off to allow rapid (< 1μs) temperature quenching [26]

181   (Fig. 1).

182   Upon temperature quenching, we found that the heated KBr had become opaque

183   to visible light when heated above 20 GPa (Fig. 2a-b). Between 13 GPa and 20 GPa, the

184   heated KBr turned a semi-transparent orange color. Owing to efficient thermal

185   conductivity of diamond, temperature gradients in the LHDAC are necessarily large.[27]

186   The absorption decreases radially outward from the laser focal spot, indicating strong

187   temperature dependence, consistent with experiments at ambient pressure that showed

188   higher F-center concentrations with increasing temperatures.[28] The resulting thickness

189   of the defect-damaged KBr was 1-2 microns, determined by interference fringes in

190   infrared reflectivity measurements. The temperature required to initiate coloration in KBr

191   increases with increasing pressure (Fig. 3). The increase in temperature required for

192   defect formation with pressure can be attributed to a greater amount of thermal energy

193   required to liberate atoms from their equilibrium positions at higher density. Because

194   there is a short (order 10 picoseconds) but finite time range between onset of defect

195   formation,[29] F-centers develop in KBr before thermal runaway is complete. Two data

196   points (Fig. 3 filled grey diamonds) demonstrate the case that defect formation began but

197   did not reach the saturation limit. This is evidenced by a smaller change of opacity than

198   samples of the same pressure that underwent complete thermal runaway and a thermal

199   emission profile that did not saturate.

200

201   **B. Pressure-Dependent Absorption**

202   While no in-situ absorption measurements were made at high temperature due to

203   technical unfeasibility, fast laser shutoff rates (~1 μs) and a rapid change in thermal

204   emission in <1 ms strongly suggest that the coloration observed after temperature

205 quenching is inherited from defects formed at high temperatures. Absorption

206 measurements were taken in the visible and infrared wavelengths after temperature

207 quenching while the samples were still at pressure. Absorbance is found to increase with

208 increasing synthesis pressure (Fig. 4), approaching a grey body by 81 GPa.

209   The lack of absorption edges rules out the possibility of an insulator to metal

210 transition occurring in the KBr. A shift and broadening of the F absorption band is in

211 accordance with the Mollwo-Ivey relationship that predicts the peak position of the F

212 band depends primarily on the lattice constant of the host crystal.[6,30,31] The pressure

213 effect can be qualitatively explained by a decreasing energy difference between

214 electronic F-center level and conduction band with pressure, consistent with a pressure

215 induced broadening of the conduction band.

216

217   **C. Crystal Structure and The Melting Curve of KBr**

218   This rapid change in absorption and emission during laser heating has been

219 previously observed and attributed to the melting of KBr.[25] Given that the optical

220 change was the sole criterion to identify the melting point in that study, our observations

221 suggest that melting is not a prerequisite for thermal runaway. Either defect formation

222 occurs before melting, or melting and defect formation begin concurrently. Therefore, the

223 only current definitive point on the high-pressure KBr melting curve is given by shock

224 compression experiments [32] that reveal melting along the Hugoniot at 33 GPa.

225   Transparent KBr is expected to remain in the B2 cubic phase in the pressure range

226 we consider [9] and is expected to be molten at the runaway temperatures (~5000+ K) we

227 measure on the absorbing KBr according to the existing high-pressure melting curve.[25]

228   The structure of defect-damaged KBr has not been characterized at these high pressures

229   or high temperatures. In addition, tetragonal and orthorhombic phases have been

230   predicted for KCl, another potassium halide, at extreme conditions exceeding 200

231   GPa.[33] Our in-situ x-ray diffraction (XRD) measurements on KBr show no evidence of

232   phase transitions or any other unexplained diffraction peaks, indicating that the KBr

233   remained in the B2 phase or a new phase was produced in too small amounts to be

234   detected by XRD (Fig. 5). Diffraction patterns rule out the possibility of chemical

235   reactions between the KBr and the metal absorber, or dissociation of KBr as observed

236   with CsI at high pressure and high temperature.[34] No diffuse melt signal was observed,

237   suggesting that the KBr became absorbing in the solid state, or potentially as a premelting

238   effect as previously suggested.[35] In KCl, for instance, the F-center concentration

239   increases rapidly just below the melting temperature.[29] However, strong

240   recrystallization texture of B2 KBr after quenching temperature suggests that KBr did

241   melt after thermal runaway in regions that became opaque, but likely only in a small and

242   localized region (Fig. S1). To bound the temperature difference between when defect

243   formation occurs and when melting occurs would require a technique with simultaneous

244   ultrafast temperature measurement and ultrafast structural characterization.

245

246   **D. Activation of Raman Modes**

247   While XRD captures the long-range order that remains virtually unaffected,

248   Raman spectroscopy reveals symmetry breaking in the local structure. Our defect-

249   damaged KBr exhibits strong Raman-active modes at high frequencies (Fig. 6). The

250   Raman peaks become more intense and shift to lower frequencies as the sample is

251 decompressed in the B2 phase. Vibrational frequencies increase during the phase

252 transition below 2 GPa in accordance with the elastic response of the B2 to B1

253 transition.[36] At ambient pressure, the Raman signal is lost and cannot be recovered

254 upon recompression. Given that Raman spectra are robust among samples heated with

255 different metal couplers Fe, FeSi, Fe-Si9wt%, and Pt (Fig. S2), we infer that this is an

256 intrinsic KBr defect rather than due to diffusion of metal impurities into the KBr, which

257 can also break translational invariance of the lattice and induce first order Raman

258 modes.[37] For any given pressure, the Raman spectra were identical regardless of the

259 metal used. Examples of defect-damaged KBr using Pt or FeSi9wt% are shown in Fig. S2

260 for ~56 GPa and on decompression to ~4.5 GPa. The similarity in spectra, especially on

261 decompression when hysteresis effects can be large, provides compelling evidence that

262 the defect is intrinsic to KBr. This is reinforced by the observation that no new phases

263 appear in the in-situ diffraction spectra (Fig. 5). Indeed, a quick comparison between our

264 Raman spectra and that of impurity-induced Raman spectra of KBr [37] show little

265 similarities, in large part due to the broad peaks and the small frequencies (most < 100

266 cm^{-1}) they measure and our inability to measure frequencies less than 100 cm^{-1}.

267

268 **E. Stability of F-Centers**

269 　　　　Upon decompression to room pressure, KBr reverts to the B1 structure with no

270 memory of damage (Fig. 5). The color centers in KBr are annealed during

271 decompression, which is apparent throughout the Raman spectra (Fig. 6), optical images

272 (Fig. 2e), and absorbance spectra (Fig. S3). The KBr becomes progressively less opaque,

273 evolving from black above 20 GPa to a bright blue color below ~2 GPa (Fig. 2),

274 consistent with the color centers observed in lower pressure studies of KBr.[38,39] For

275 this reason, we attribute this defect state to high-pressure F-centers in KBr. This is in

276 contrast with early work that observed an increase in absorption energy of the F-center in

277 KBr with pressures to ~15 GPa and predicted a continual increase in the absence of a

278 phase transition.[3,4] These studies generated F-centers at room pressure and temperature

279 conditions using x-irradiation, and defected samples were subsequently taken to pressures

280 much lower than those achieved in our study. The thermal energies of these LHDAC

281 experiments exceed 0.43 eV (nominal T= 5000 K). This is comparable to the energy

282 range used in recent short-lived F-center studies using other defect-forming

283 techniques.[1,2,40,41] The absence of an XRD signal from the defects and the presence

284 of Raman peaks indicate that the defects are localized to the heated region. In our DFT

285 calculations, we relax KBr F-centers in the B1 and B2 phases and confirm that structural

286 distortions are very small, consistent with previous work.[17] Furthermore, symmetry

287 analysis of the computationally relaxed structures shows that the resulting structures can

288 be described within the same space group as B2, consistent with our XRD observations.

289 The number of Raman modes observed in our study is consistent with previous

290 observations in the B1 KBr phase that have been attributed to F-centers.[37] Previous

291 work finds that optical F-band absorption energy, attributed to the 1s-to-2p transition,[42]

292 increases with decreasing volume (increasing pressure).[6] With increasing pressure, the

293 conduction bandwidth and F-center transition energies increase which suggests that

294 during relaxation after the optical excitation, a larger amount of energy can be converted

295 to phonons, consistent with the runaway heating observed experimentally.

296   While F-centers in KBr have shown to be stable in the range of microseconds

297   [40,43] to a year,[39] we have observed the stability of the defects through sustained

298   coloration for greater than 1 month prior to decompression. If left under pressure,

299   lifetimes may be much longer. A recent study that observed comparatively long stability

300   timescales of one year for color centers in KBr required femtosecond laser pulse energies

301   of 31-156 GeV [39] and observed increasing defect density with increasing energy, in

302   concordance with our observations. At 68 GPa, a combined pressure-volume and thermal

303   energy of ~30 eV was sufficient to stabilize defects for a minimum of one month.[44]

304   The Raman vibrational spectra suggest a strong pressure dependence of the stability and

305   optical properties of F-centers and leave the aspect of time as an open area of future

306   research.

307

308   **IV. APPLICATION TO TEMPERATURE CORRECTION**

309   Accurate temperature measurements at high pressure have been a difficult task

310   throughout the history of laser heating.[45] While progress has been made in careful

311   temperature measurements, the contribution of wavelength-dependent absorption has

312   only recently been considered.[46] KBr and other salts are frequently used as insulation

313   in LHDAC experiments under the assumption that they remain transparent in the visible

314   wavelength range. Noble gases are used as insulation for similar reasons, but they also

315   become opaque at high pressures and temperatures.[47] Most laser heating is performed

316   in a hutch at a synchrotron, so temporal evolution of heating is difficult to monitor.

317   Additionally, heating is typically performed with KBr overlying opaque materials so that

318   a change in KBr color is not distinguishable from sample color or changes in sample

319 color. For these reasons, the absorbing behavior in salts at extreme conditions is not well

320 documented despite potential issues in LHDAC experiments. Wavelength-dependent

321 absorption (Fig. 4) due to defects may cause temperature deviations of hundreds to

322 thousands of degrees, resulting in incorrectly interpreted temperatures [46](Fig. 7, 8).

323   We measure temperature using 4-color multi-wavelength imaging

324 radiometry.[10] Intensity of light from the sample is measured at 4 wavelengths: 580 nm,

325 640 nm, 766 nm, and 905 nm in the area of the hotspot, and we use a Wien fit to obtain a

326 two-dimensional map of the apparent temperature (T_a) as shown in Fig. 7. In the case of a

327 transparent insulation medium overlying a blackbody laser absorber, the apparent

328 temperature is nearly equal to the real temperature (T_r). In the case that either the

329 insulation medium or the laser absorber has variable wavelength-dependent absorption,

330 $T_a \neq T_r$, and a temperature correction is required,[46] as shown for 4 specific samples of

331 color center-defected KBr in Fig. 8. Fig. 7 shows a hotspot measured while KBr began to

332 absorb the laser. While the laser is ramped to a peak power and held steady, the thermal

333 emission begins to rapidly increase once defect formation begins (Fig. 1). Lineout

334 intensity profiles measured at four different wavelengths reveal intensities that decrease

335 radially outward so that temperature should also decrease radially outward. Upon

336 inspection of the temperature map, this does not hold throughout the hotspot when fit to a

337 uniform blackbody spectrum. At 22 GPa, the absorption profile in the center of the

338 hotspot absorbs more at shorter wavelengths (Fig. 4), causing a higher apparent

339 temperature than the sample truly experiences. Moving outward from the center of the

340 hotspot in Fig. 7, large temperature gradients correspond to drastic changes in defect

341 concentration, or opacity. The wavelength-dependent absorption profile changes

342 significantly moving outward from the hotspot, leading to apparent higher temperatures

343 at the edge of the hotspot, which is unphysical and inconsistent with the monotonically

344 decreasing intensities.

345   Even with the temperature correction shown, it is noted that T_r is representative of

346 the temperature of the KBr and not the temperature of the laser absorber. Once the KBr

347 forms an absorbing layer, the metal becomes poorly insulated. To obtain the temperature

348 of the laser absorber in order to correct previous melting curves, for instance, the KBr can

349 not be opaque. If the KBr is semitransparent, then extensive thermal modeling based on

350 sample geometry is required to determine the temperature of the laser absorber and is left

351 for future work. Else, if the KBr becomes opaque, the temperature measured will be

352 approximately the temperature of KBr with minimal temperature correction. Fig. 8 shows

353 the deviation of apparent temperature (T_a) from real temperature (T_r) in optical thickness

354 space, with T_r being the maximum temperature reached by the 22 GPa sample in Fig. 4.

355 The optical thickness τ_λ is given by $\tau_\lambda = \int_0^d k_\lambda dz$ where k_λ is the absorption coefficient

356 at wavelength λ and d is the thickness of the material that participates in radiative heat

357 transfer at wavelength λ. For this scenario, d is the thickness of the resulting defect-

358 damaged KBr. At 22 GPa, the correction is drastic. The temperature map collected prior

359 to any temperature correction due to wavelength-dependent absorption (Fig. 4), yields a

360 peak temperature of ~8100 K (Fig. 7), which is ~2600 K greater than the real temperature

361 of 5500 K (Fig. 8). When defects are generated at higher pressures such as at 81 GPa, the

362 grey body assumption becomes valid once more (Fig. 4), so that the measured

363 temperature of the defected KBr itself is valid, noting that it is the defected KBr

364 temperature that is being measured rather than the underlying sample. Characterizing

365 high-pressure, high-temperature defect properties may offer an explanation for highly

366 contested data sets such as the high-pressure melting curve of iron. The experimental

367 melting curve of iron, though studied for decades, still shows discrepancies of ~1000 K

368 when extrapolated to Earth's inner-core boundary pressure of ~330 GPa [48-50]. Defect-

369 related optical changes in the alkali halides used to insulate the iron may provide an

370 explanation for these observed large discrepancies and directly affect our understanding

371 of the evolution of our planet.

372

373   **V. CONCLUSIONS**

374   We observe a wide range of thermally-induced coloration in KBr in the LHDAC

375 based on synthesis pressure. While in-situ XRD reveals no significant change in bulk

376 structure, emergence of strong Raman modes and wavelength-dependent absorption in

377 the initially transparent KBr indicate the generation of F-centers at high pressure and

378 temperature. When held at pressure, annealing of defects is stalled compared to room

379 pressure studies, with coloration persisting for at least one month. Since diamonds are

380 opaque to UV radiation and defects are annealed on decompression, the ability to probe

381 excitonic features in the LHDAC is limited. Otherwise, photoluminescence spectroscopy

382 and UV absorption would aid in confirming this phenomenon and determining the

383 electronic signature of the defect state. While it is not possible to determine if KBr

384 melting occurs just prior to, concurrent with, or just after thermal runaway with our

385 measurements, it is possible to conclude the simultaneity of defect formation with

386 thermal runaway. While the observation of thermal runaway was previously used to infer

387 onset of melting of KBr at high pressures,[25] this study concludes that defect formation

388 is the physical cause of observed thermal runaway but is still a good indicator of melting

389 within high-pressure temperature measurement errors. If amorphous melt diffraction can

390 be identified while monitoring finely time-resolved thermal emission, this would provide

391 a diagnostic to determine whether the defect formation occurs before, during, or after

392 melting of KBr.

393   While we direct our attention to the coloration of KBr at high pressures and

394 temperatures, we note that the runaway temperature effect due to defect formation is

395 likely a robust phenomenon for all alkali halides. In a few separate experiments (Table I),

396 we observed similar color changes in NaCl, KCl, and CsCl at high pressures. Because of

397 the ubiquitous use of KBr and other alkali halides in LHDAC experiments as insulation

398 and/or as a pressure medium/calibration standard [51], its coloration at high pressures and

399 temperatures is of special concern to our understanding of high-energy density physics.

400

420

421

422

423

424   **FIG. 1.** A representative evolution of laser power (dark grey curve), thermal emission

425   while heating versus time for a sample without defect formation (light grey thin curve),

426   and thermal emission while heating versus time for a saturated defect formation sample

427   e.g., FeSi954s2 (black thick curve). For the defect-saturated sample, runaway heating

428   begins at ~3700 ms, and goes from relatively steady heating to runaway in <1 ms (the

429   time resolution of the photodiode). For the defect-free sample, emission plateaus at the

430   peak power.
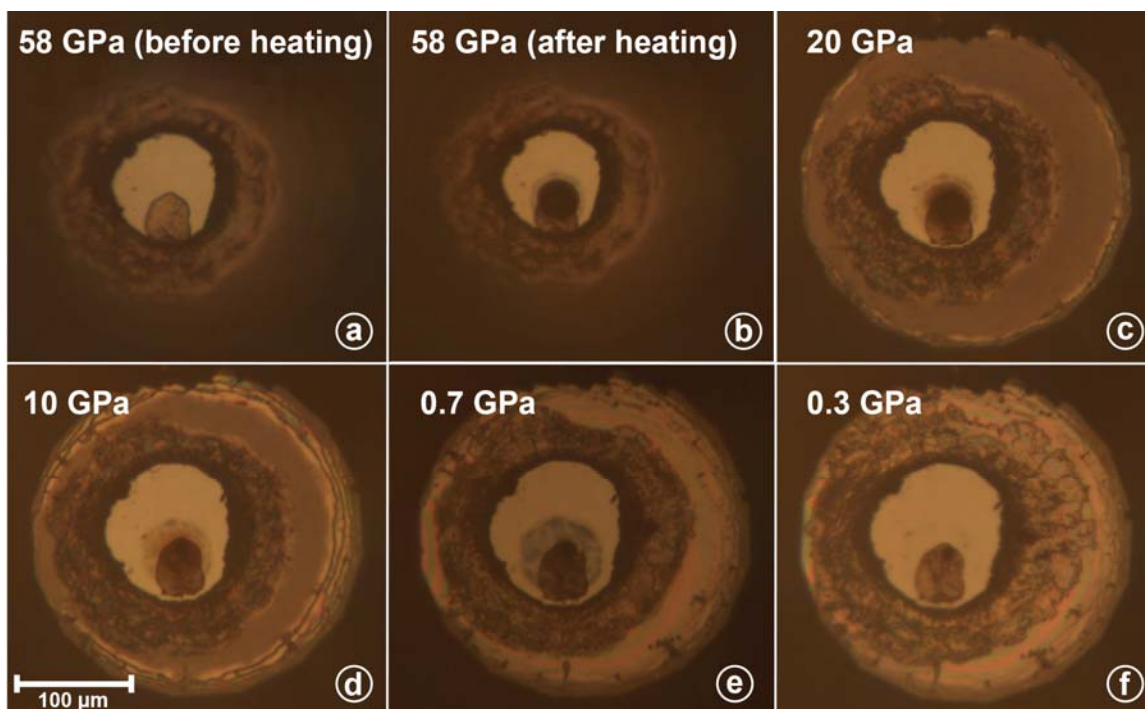
FIG. 2. Optical images of defect-damaged KBr02s1 during decompression. Images were taken while at pressure in a LHDAC using both reflected and transmitted light. **(a)** Before heating, only the metal foil, used as a laser absorber, is visible in the gasket hole, surrounded by transparent KBr. **(b)** When heated on the tip of the metal foil, the KBr becomes absorbing, and the entire heated region of KBr darkens. **(c-f)** Upon decompression, the defect-damaged KBr becomes less absorbing, progressing from black to orange, to blue after the B2 to B1 phase transition at ~1.8 GPa, and eventually returning to transparent at room pressure.

440
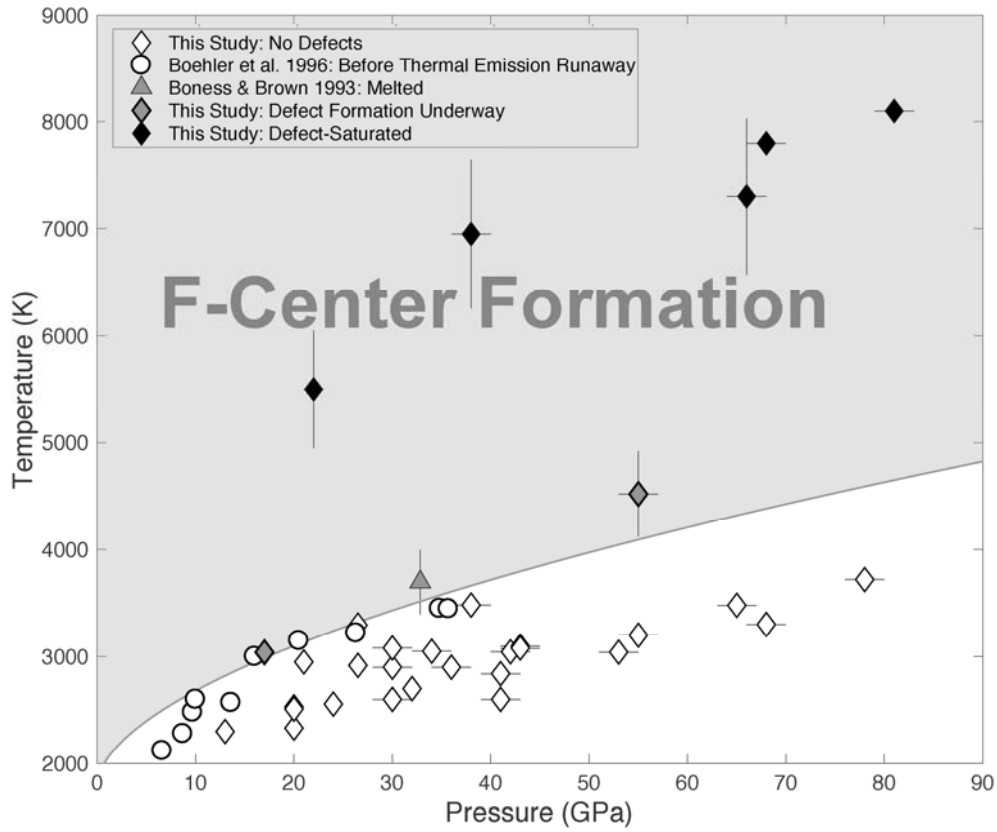
FIG. 3. Estimated temperatures required for the onset of rapid F-center formation in KBr

at high pressures. At the curve, runaway heating begins, and above the curve, F-centers

are present in KBr. Diamond symbols are temperature measurements from this study.

Error bars for open diamonds are of the same size or smaller than the symbols ($\leq \pm 100$

K). Circles [25] represent the last temperature measured before thermal runaway. The

grey triangle [32] from a shock study pins down the melting temperature of KBr. Open

symbols represent measurements of KBr in which no defects were observed, and filled

symbols represent defect formation underway (grey symbols) and defect-saturated (black

symbols) samples. The curve is speculative and fit using previous data [25] as a tight

lower bound to onset of defect formation up to ~36 GPa together with our measurements

at 17 GPa and 55 GPa as upper bounds to the onset of defect formation.

452
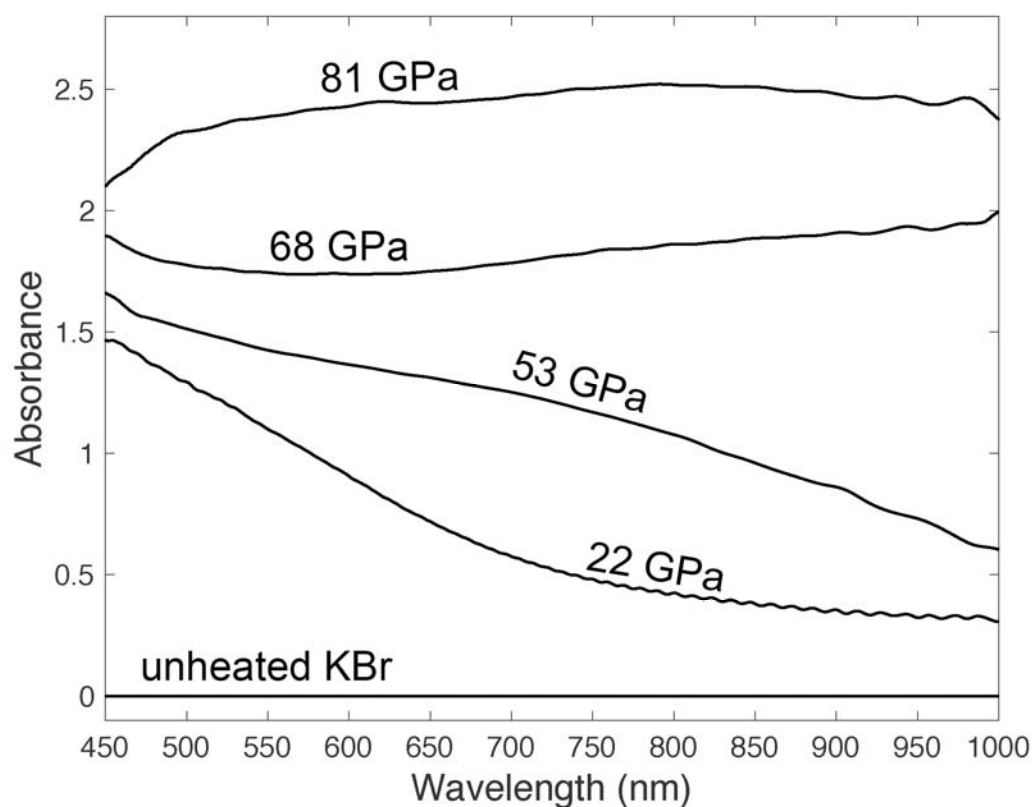
FIG. 4. High-pressure visible absorbance spectra for defect-damaged KBr samples

(KBr07s1, FeSi923s1, KBr08s2, KBr10s1) after quenching from high temperature. The

thickness of the defect-damaged region is 1 μm. Unheated and un-defected KBr,

regardless of the pressure, remains transparent in the wavelength range considered.

457
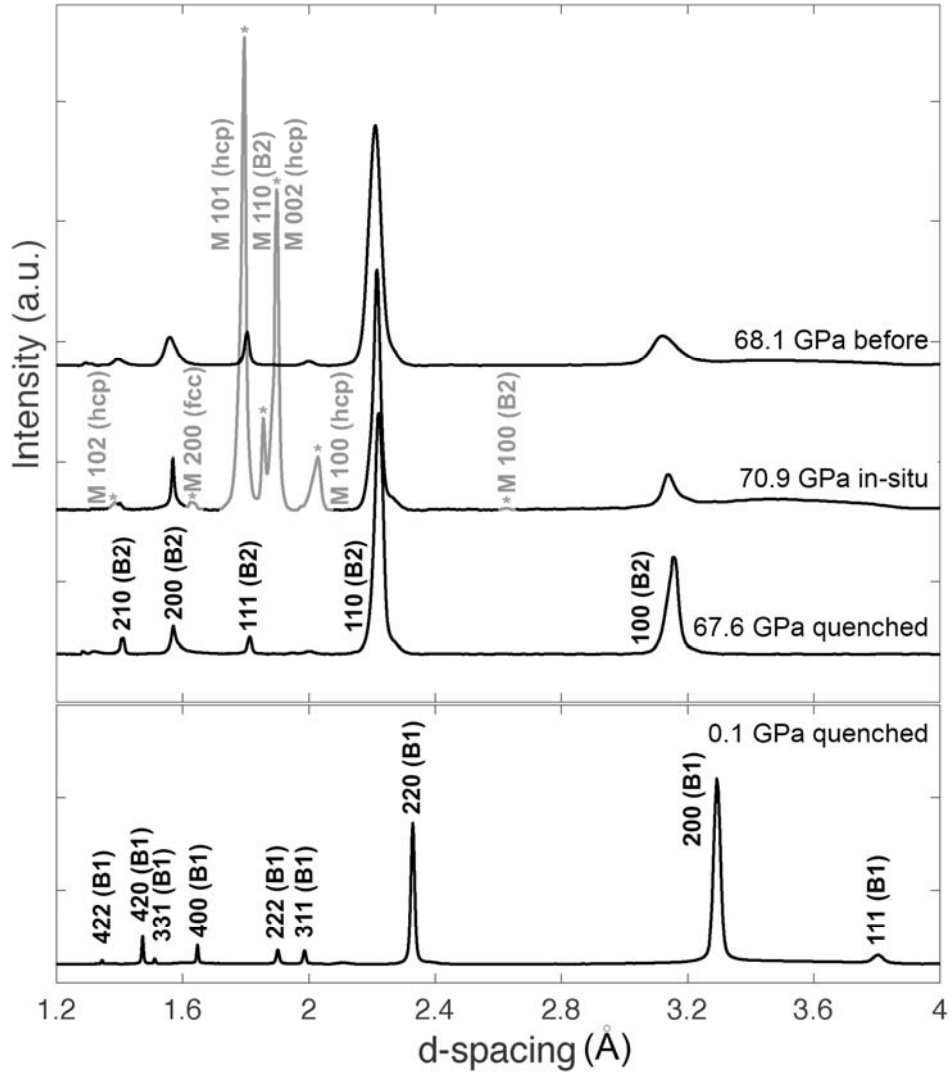
FIG. 5. **(Top)** XRD pattern taken at 68.1 (± 0.1) GPa before heating, 70.9 (± 0.1) GPa

during runaway heating to ~8000 K, and after heating at 67.6 (±0.1) GPa on the darkened

defect-damaged sample KBr11s1. Grey peaks with asterisks and labeled M correspond to

hcp, B2, and fcc Fe-Si9wt% solid phases of the metal coupler. KBr remains structurally

closed with respect to the B2 phase during defect formation. Despite the high

temperatures while in thermal runaway, the FeSi9wt% metal coupler remains in its solid

state. **(Bottom)** XRD pattern of KBr quenched to near room pressure that has reverted

back to the B1 phase. See also Figure S1 for raw data.

466
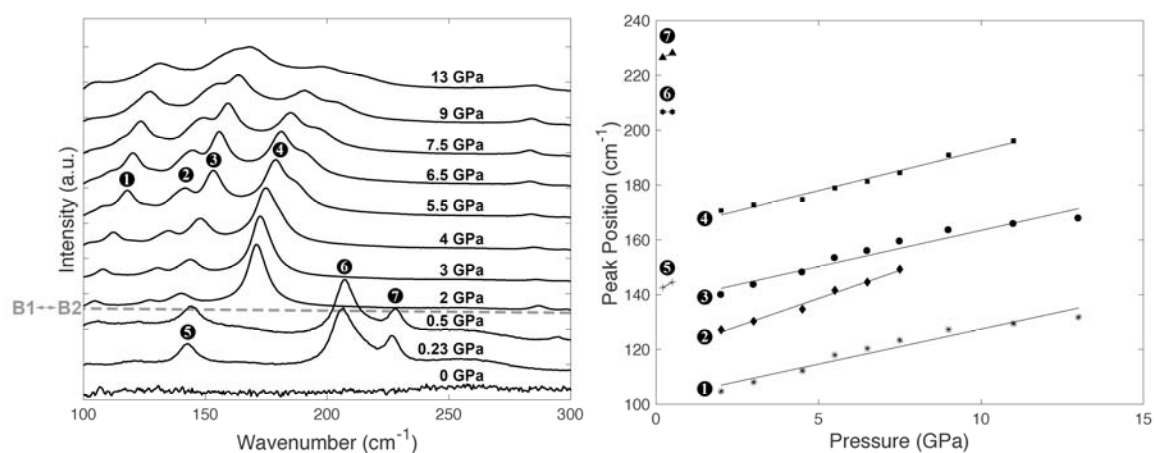
467 **FIG. 6 (Left**) Raman spectra of defect-damaged sample KBr01s3 synthesized at 13 GPa

468 on decompression. Horizontal dashed line corresponds to the B1→ B2 phase boundary,

469 which occurs at pressures < 2 GPa. **(Right)** Evolution of peak frequencies with pressure

470 during decompression.

471
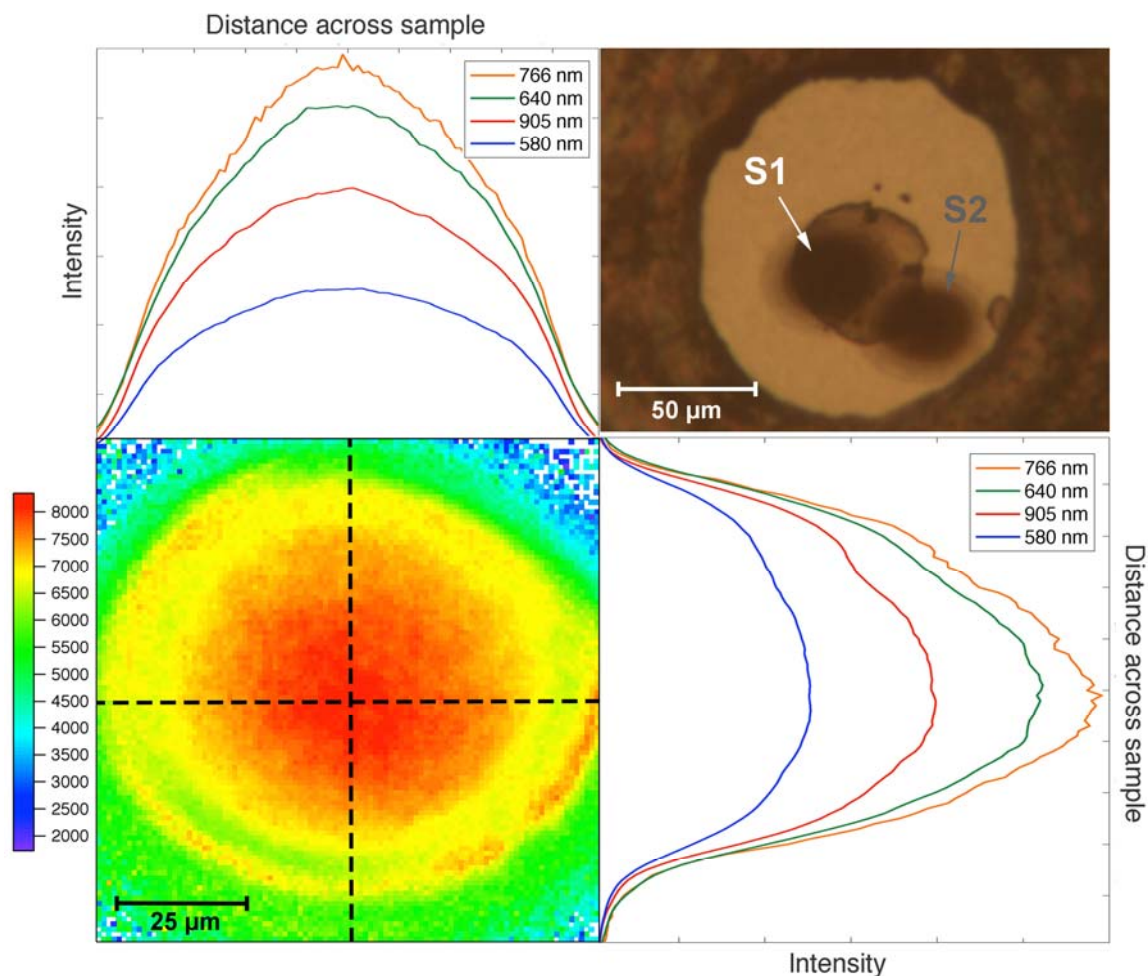
FIG. 7. Uncorrected 2D temperature map for a defect-damaged sample KBr07s1 at 22

GPa. Upper left and lower right: Horizontal and vertical intensity profiles along the

dashed transects marked on the temperature map. Upper right: optical image showing two

heated and defect-damaged spots using both reflected and transmitted light.
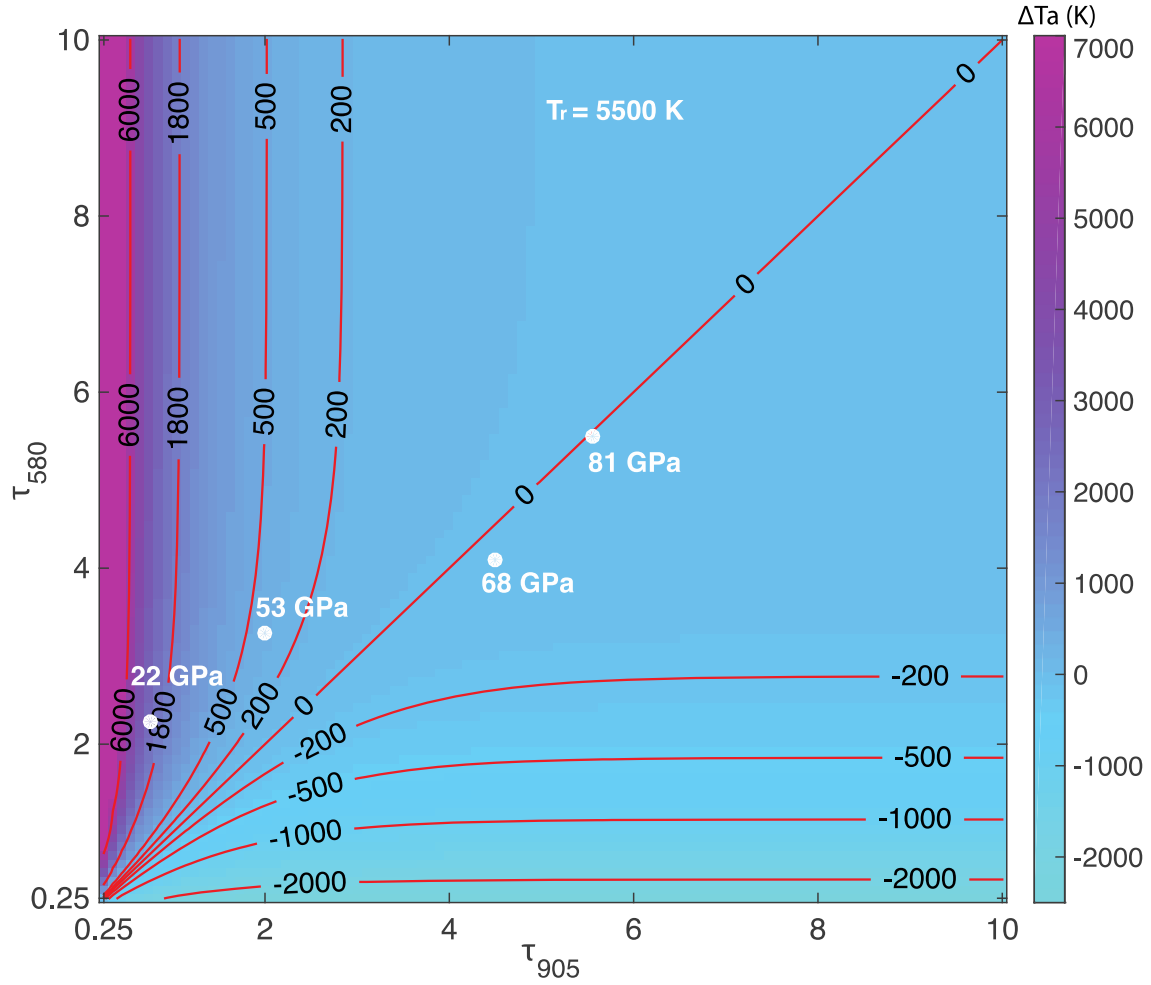
FIG. 8. Effect of wavelength-dependent absorption from defect-damaged KBr on

temperature measurements at a nominal maximum real temperature of 5500 K (see [46]

for more details). The axes represent optical thickness at 580 nm and 905 nm,

respectively for an absorbing hotspot 1 μm in thickness. The color gradient and

corresponding contours show the deviation of apparent measured temperature from the

real temperature (T_a-T_r). Thus, for **Fig. 7**, the sample at 22 GPa has a measured peak

temperature in excess of 8000 K. However, due to the strong wavelength-dependent

absorbing nature of a sample heated at those pressures, the real temperatures is ~5500 K,

which is 2600 K lower than what was measured.

486   **Table I.** Experiment parameters for all samples in which defect formation was observed.

487   Sample details include the alkali halide sample, metal coupler used for laser heating as

488   well as cook time in oven at ~400 K to minimize any moisture in the sample. Pressure

489   listed is based on the high-frequency edge of the diamond Raman band [8] and is the

490   pressure measured after heating. Uncertainties in pressure are determined by the

491   measured pressure gradients [51]. The sample is single-sided laser heated subjected to

492   either steady heating or predefined ramp heating [10], in which the sample is annealed at

493   a low laser power (first power listed below) for a set amount of time (first heating

494   duration value listed below) and subsequently ramped to a peak power (second power

495   listed below) for one second and held constant for the remainder of the heating cycle (last

496   time listed). For example, FeSi936 is annealed at a low laser power of 30 W for 2

497   seconds, then ramped to 100 W between 2-3 seconds and then held at 100 W from 3-4

498   seconds. If only one parameter is listed, ramped heating was not used. Not all samples

499   listed here appear in **Fig. 3** due to either saturation of the charge-coupled detector (CCD),

500   which collected the light for temperature measurement, or lack of absorption data for a

501   temperature correction. For these saturated or uncorrected samples, the temperature

502   listed is NA (not available). Sample names with asterisks are those with temperatures

503   taken just as thermal runaway was beginning and are depicted as grey diamonds in **Fig. 3**.

Sample Name/ Spot Number	Sample Material	Metal Coupler	Pressure (GPa)	Temperature of defect formation (K)	Laser Power (W)	Heating Duration (s)	Cook Time in Oven
KBr01s2	KBr	Fe-Si9wt%	13 ± 1	NA	30	6	1 hour
KBr01s3	KBr	Fe-Si9wt%	13 ± 1	NA	30	6	1 hour
KBr02s1	KBr	Fe-Si9wt%	60 ± 2	NA	70	6	1 hour
KBr03s1	KBr	Pt	55 ± 2	NA	50	6	1 hour
KBr04s1	KBr	Fe	37 ± 2	7000 ± 700	40	6	1 hour
KBr04s2	KBr	Fe	37 ± 3	7000 ± 700	43	6	1 hour

KBr04s3	KBr	Fe	37 ± 2	7000 ± 700	45	6	1 hour
KBr05s1	KBr	FeSi	66 ± 2	7300 ± 730	90	6	3.5 hours
KBr07s1	KBr	Fe-Si9wt%	22 ± 1	5500 ± 550	60	6	1 hour
KBr07s2	KBr	Fe-Si9wt%	22 ± 1	5500 ± 550	60	6	1 hour
KBr08s2	KBr	FeSi	68 ± 2	7800 ± 100	75	6	1 hour
KBr09s1	KBr	Fe-Si9wt%	32 ± 1	NA	50	6	1 hour
KBr09s2	KBr	Fe-Si9wt%	32 ± 1	NA	50	6	1 hour
KBr10s1	KBr	Fe-Si9wt%	81 ± 2	8100 ± 100	85	6	1 hour
KBr11s1	KBr	Fe-Si9wt%	68 ± 3	NA	100	2	none
FeSi921s1*	KBr	Fe-Si9wt%	55 ± 2	4500 ± 450	50	6	1 hour
FeSi922s1	KBr	Fe-Si9wt%	54 ± 2	NA	65	6	1.5 hours
FeSi922s2	KBr	Fe-Si9wt%	54 ± 2	NA	72	6	1.5 hours
FeSi923s1	KBr	Fe-Si9wt%	53 ± 2	NA	70	2-3-4 ramped	1 hour
FeSi935s1	NaCl	Fe-Si9wt%	15 ± 1	NA	27-39 ramped	2-3-4 ramped	10 days
FeSi935s2	NaCl	Fe-Si9wt%	15 ± 1	NA	27-38 ramped	2-3-4 ramped	10 days
FeSi936s1	NaCl	Fe-Si9wt%	58 ± 2	NA	60-90 ramped	2-3-4 ramped	1 hour
FeSi938s4	CsCl	Fe-Si9wt%	50 ± 2	NA	17-45 ramped	2-3-4 ramped	1 hour
FeSi939s2	KCl	Fe-Si9wt%	45 ± 2	NA	30-50 ramped	2-3-4 ramped	1 hour
FeSi942s2	KBr	Fe-Si9wt%	13 ± 1	NA	13-26 ramped	2-3-4 ramped	1 hour
FeSi948s1	KBr	Fe-Si9wt%	22 ± 1	NA	11-22 ramped	2-3-4 ramped	1 hour
FeSi954s2	KBr	Fe-Si9wt%	32 ± 2	NA	22-46 ramped	2-3-4 ramped	1 hour
FeSi954s3	KBr	Fe-Si9wt%	32 ± 2	NA	22-45 ramped	2-3-4 ramped	1 hour
FeSi955s1*	KBr	Fe-Si9wt%	17 ± 1	3000 ± 100	15-26 ramped	2-3-4 ramped	1 hour
FeSi964s1	KBr	Fe-Si9wt%	48 ± 3	NA	21-61 ramped	2-3-4 ramped	1 hour
FeSi964s2	KBr	Fe-Si9wt%	48 ± 3	NA	21-48 ramped	2-3-4 ramped	1 hour
FeSi966s4	KBr	Fe-Si9wt%	20 ± 1	NA	10-26 ramped	2-3-4 ramped	14 hours
FeSi968s2	KBr	Fe-Si9wt%	36 ± 2	NA	17-36 ramped	2-3-4 ramped	1 hour
FeSi974s2	KBr	Fe-Si9wt%	30 ± 1	NA	20-42 ramped	2-3-4 ramped	1 hour

| FeSi974s3 | KBr | Fe-Si9wt% | 30 ± 1 | NA | 20-41 ramped | 2-3-4 ramped | 1 hour |
| FeSi982s2 | KBr | Fe-Si9wt% | 65 ± 3 | NA | 32-79 ramped | 2-3-4 ramped | 14 hours |

504

505

Table II: DFT computed F-center formation energies for single atom defects in KBr.

Phase	Pressure (GPa)	Br-poor (F-center) (eV)	K-poor (eV)
B1	0	0.4	1.2
B2	0	0.5	0.5
B2	50	1.9	3.6

507

508

References

510 [1]   F. Seitz, Rev Mod Phys **18**, 384 (1946).
511 [2]   C. R. A. Catlow, K. M. Diller, and L. W. Hobbs, Philos Mag A **42**, 123 (1980).
512 [3]   W. G. Maisch and H. G. Drickamer, J Phys Chem Solids **5**, 328 (1958).
513 [4]   R. A. Eppler and H. G. Drickamer, J Chem Phys **32**, 1418 (1960).
514 [5]   I. S. Jacobs, Phys Rev **93**, 993 (1954).
515 [6]   C. J. Buchenauer and D. B. Fitchen, Phys Rev **167**, 846 (1968).
516 [7]   M. J. Poston, R. W. Carlson, and K. P. Hand, Journal of Geophysical Research:
517 Planets , 122, 2017).
518 [8]   Y. Akahama and H. Kawamura, International Conference on High Pressure
519 Science and Technology, Joint Airapt-22 and Hpcj-50 **215** (2010).
520 [9]   A. Dewaele, A. B. Belonoshko, G. Garbarino, F. Occelli, P. Bouvier, M.
521 Hanfland, and M. Mezouar, Phys Rev B **85** (2012).
522 [10]   Z. X. Du, G. Amulele, L. R. Benedetti, and K. K. M. Lee, Rev Sci Instrum **84**
523 (2013).
524 [11]   Y. Meng, G. Shen, and H. K. Mao, J Phys-Condens Mat **18**, S1097 (2006).
525 [12]   G. Kresse and J. Furthmuller, Comp Mater Sci **6**, 15 (1996).
526 [13]   G. Kresse and J. Furthmuller, Phys Rev B **54**, 11169 (1996).
527 [14]   J. P. Perdew, K. Burke, and M. Ernzerhof, Phys Rev Lett **77**, 3865 (1996).
528 [15]   G. Kresse and D. Joubert, Phys Rev B **59**, 1758 (1999).
529 [16]   P. E. Blochl, Phys Rev B **50**, 17953 (1994).
530 [17]   W. Chen, C. Tegenkamp, H. Pfnur, and T. Bredow, Phys Rev B **82** (2010).
531 [18]   F. SEITZ, Rev Mod Phys **26**, 7 (1954).
532 [19]   A. San-Miguel, H. Libotte, M. Gauthier, G. Aquilanti, S. Pascarelli, and J. P.
533 Gaspard, Phys Rev Lett **99** (2007).
534 [20]   P. K. de Boer and R. A. de Groot, Eur Phys J B **4**, 25 (1998).

535 [21]   F. C. Brown, C. Gahwiller, H. Fujita, A. B. Kunz, W. Scheifley, and N. Carrera,
536 Phys Rev B-Solid St **2**, 2126 (1970).
537 [22]   D. Grojo, S. Leyder, P. Delaporte, W. Marine, M. Sentis, and O. Uteza, Phys Rev
538 B **88** (2013).
539 [23]   M. Shishkin and G. Kresse, Phys Rev B **75** (2007).
540 [24]   C. Adamo and V. Barone, J Chem Phys **110**, 6158 (1999).
541 [25]   R. Boehler, M. Ross, and D. B. Boercker, Phys Rev B **53**, 556 (1996).
542 [26]   Z. Du, J. Deng, and K. K. M. Lee, *under*
543 *review at Geophysical Research Letters* (2017).
544 [27]   W. Panero and R. Jeanloz, J Geophys Res **106**, 6493 (2001).
545 [28]   J. D. Comins, Phys Status Solidi B **43**, 101 (1971).
546 [29]   R. Williams, J. Bradford, and W. Faust, Phys Rev B **18**, 7038 (1978).
547 [30]   H. F. Ivey, Phys Rev **72**, 341 (1947).
548 [31]   P. Tiwald, F. Karsai, R. Laskowski, S. Grafe, P. Blaha, J. Burgdorfer, and L.
549 Wirtz, Phys Rev B **92** (2015).
550 [32]   D. A. Boness and J. M. Brown, Phys Rev Lett **71**, 2931 (1993).
551 [33]   A. Shamp, P. Saitta, and E. Zurek, Phys Chem Chem Phys **17**, 12265 (2015).
552 [34]   Q. Williams and R. Jeanloz, Phys Rev Lett **59**, 1132 (1987).
553 [35]   J. L. Tallon, W. H. Robinson, and S. I. Smedley, J Phys Chem-Us **82**, 1277
554 (1978).
555 [36]   A. M. Hofmeister, Phys Rev B **56**, 5835 (1997).
556 [37]   B. N. Ganguly and M. Nicol, J Appl Phys **47**, 2467 (1976).
557 [38]   H. Sothe, J. M. Spaeth, and F. Luty, J Phys-Condens Mat **5**, 1957 (1993).
558 [39]   X. W. Wang, R. Buividas, F. Funabiki, P. R. Stoddart, H. Hosono, and S.
559 Juodkazis, Appl Phys a-Mater **122** (2016).
560 [40]   J. T. Dickinson, S. C. Langford, S. M. Avanesyan, and S. Orlando, Appl Surf Sci
561 **253**, 7874 (2007).
562 [41]   D. W. Lynch and D. A. Robinson, Phys Rev **174**, 1050 (1968).
563 [42]   J. H. Simpson, Proc R Soc Lon Ser-A **197**, 269 (1949).
564 [43]   R. K. Swank and F. C. Brown, Phys Rev **130**, 34 (1963).
565 [44]   See Supplemental Material at [URL will be inserted by publisher] for
566 experimental details and supplemental figures.
567 [45]   R. Jeanloz and A. Kavner, Philos T R Soc A **354**, 1279 (1996).
568 [46]   J. Deng, Z. Du, L. R. Benedetti, and K. K. M. Lee, J Appl Phys **121**, 025901
569 (2017).
570 [47]   R. S. McWilliams, D. A. Dalton, Z. Konopkova, M. F. Mahmood, and A. F.
571 Goncharov, P Natl Acad Sci USA **112**, 7925 (2015).
572 [48]   R. Boehler, D. Santamaria-Perez, D. Errandonea, and M. Mezouar, J Phys Conf
573 Ser **121** (2008).
574 [49]   S. Anzellini, A. Dewaele, M. Mezouar, P. Loubeyre, and G. Morard, Science **340**,
575 464 (2013).
576 [50]   J. M. Jackson *et al.*, Earth Planet Sc Lett **362**, 143 (2013).
577 [51]   I. Uts, K. Glazyrin, and K. K. M. Lee, Rev Sci Instrum **84** (2013).
578